## A KINETIC APPROACH TO ACTIVE RODS DYNAMICS IN CONFINED DOMAINS\*

LEONID BERLYAND<sup>†</sup>, PIERRE-EMMANUEL JABIN<sup>‡</sup>, MYKHAILO POTOMKIN<sup>†</sup>, AND ELŻBIETA RATAJCZYK<sup>†</sup>§

Abstract. The study of active matter consisting of many self-propelled (active) swimmers in an imposed flow is important for many applications. Self-propelled swimmers may represent both living and artificial ones such as bacteria and chemically driven bimetallic nanoparticles. In this work we focus on a kinetic description of active matter represented by self-propelled rods swimming in a viscous fluid confined by a wall. It is well known that walls may significantly affect the trajectories of active rods in contrast to unbounded or periodic containers. Among such effects are accumulation at walls and upstream motion (also known as negative rheotaxis). Our first main result is the rigorous derivation of boundary conditions for the active rods' probability distribution function in the limit of vanishing inertia. Finding such a limit is important because (i) in many examples of active matter inertia is negligible, since swimming occurs in the low Reynolds number regime, and (ii) this limit allows us to reduce the dimension—and so computational complexity—of the kinetic description. For the resulting model, we derive the system in the limit of vanishing translational diffusion which is also typically negligible for active particles. This system allows for tracking separately active particles accumulated at walls and active particles swimming in the bulk of the fluid.

Key words. active matter, multiscale, Fokker-Planck

AMS subject classifications. 35Q84, 35Q92

**DOI.** 10.1137/19M1263510

1. Introduction. Recently, active matter has attracted much attention from the scientific community (see, e.g., reviews [7, 21, 33]). In general, active matter is defined as a system of many agents moving due to consumption of energy stored in the surrounding environment (e.g., chemical or food) and converting it into mechanical force which is called *self-propulsion*. The agents exhibiting self-propulsion are named active, as opposed to passive agents which can move only if an external field is applied. There are a vast number of examples of active matter, from suspensions of bacteria [13, 14, 15, 18, 20, 32, 37], flocks of birds [5, 25, 30], and schools of fish [19, 40] to crowds of people [29] which also meet the definition of active matter since people exhibit self-propulsion (walking). Modeling and further analysis of active matter are of great importance due to the variety of striking phenomena and promising applications (reduction of viscosity, cargo delivery for medical purposes, materials repair, etc.).

In this work, we are interested in modeling the wide class of active matter where agents are rod-shaped microswimmers, i.e., the surrounding environment is a viscous fluid and swimming occurs in the low Reynolds number regime. Examples of

<sup>\*</sup>Received by the editors May 23, 2019; accepted for publication (in revised form) October 23, 2019; published electronically January 2, 2020.

https://doi.org/10.1137/19M1263510

**Funding:** The work of the first, third, and fourth authors was supported by NSF DMREF grant DMS-1628411. The work of the second author was partially supported by NSF grants 1614537, 1908739, and RNMS (Ki-Net) 1107444.

<sup>&</sup>lt;sup>†</sup>Department of Mathematics, Pennsylvania State University, University Park, PA 16802 (lvb2@psu.edu, mup20@psu.edu).

 $<sup>^{\</sup>ddagger} Department$  of Mathematics, University of Maryland, College Park, MD 20742-3289 (pjabin@cscamm.umd.edu).

<sup>§</sup>Department of Mathematics, Faculty of Electrical Engineering and Computer Science, Lublin University of Technology, Nadbystrzycka 38A, 20-618 Lublin, Poland (elaratajczyk@onet.pl).

such microswimmers are bacteria (especially rod-shaped *Bacillus subtilis*) and active bimetallic micro- and nanorods which swim in a viscous solution with hydrogen peroxide [27]. It was observed both theoretically and experimentally for various types of microswimmers that their trajectories are much more complex than in the case of passive swimmers which simply follow streamlines of an external field (the background flow). In particular, the following phenomena were observed in dynamics of active microswimmers: accumulation at walls (bordertaxis) and upstream motion (rheotaxis); see [1, 2, 3, 9, 10, 16, 26, 31, 32, 34, 35, 42, 45] and references therein. Throughout the paper we use the term "active rods" for these rod-shaped active microswimmers.

There are two common mathematical approaches to describe dynamics of an active rod in a viscous fluid. The first one is based on force and torque balances for each individual active rod. This approach results in a Langevin equation (or a system of coupled Langevin equations) for unknown location, orientation, and velocities, both translational and angular, of the active rod. In the second approach, which is also called a kinetic approach, the main unknown is the probability distribution function of the active rod, and the function satisfies the Fokker–Planck equation. These two approaches are directly related mathematically: roughly speaking, the right-hand sides of equations in the first approach are coefficients of the Fokker–Planck equation in the second approach. The second approach is more preferable if one studies statistical properties of a large number of active rods since it does not require many realizations, unlike the first direct one.

The focus of this work is on the development of a kinetic approach for active rods swimming in a container restricted by a confinement (a wall). One can formulate how an active rod behaves when it collides with the wall (a collision rule) in the first approach. On the other hand, it is not immediately clear how the collision rule translates into a boundary condition for the Fokker–Planck equation. This is because a collision rule is typically a relation between velocities before and after a collision, whereas the Fokker–Planck equation is usually written in the vanishing inertia (overdamped) limit. Thus, the active rods' velocities are no longer variables of the unknown probability distribution function. The vanishing inertia limit of the Fokker–Planck equation is relevant for the low Reynolds number regime and important since it allows one to reduce dimension and thus drastically decrease computational complexity and even make the equation amenable for analysis.

Our first result is the rigorous derivation of this limit and, more importantly, the boundary condition for the overdamped Fokker–Planck equation in this limit. Namely, we show that the limiting probability distribution function, which depends on the active rod's location and orientation, satisfies the no-flux condition on the wall for each given orientation. We note that similar boundary conditions were phenomenologically and independently derived in [8] to analyze the distribution of active rods inside an infinite channel.

Next, we consider the case of a small translational diffusion which is negligible in experiments for active particles and equated to zero in corresponding individual based models. By using the boundary layer multiscale approach, we derive the kinetic system in the limit of vanishing translational diffusion. The significance of the system is that it describes explicitly the population of active rods accumulated at walls.

The structure of this paper is as follows. First, in section 2 we formulate our two main results on vanishing inertia and vanishing translational diffusion limits. Details of the results' derivation are relegated to sections 3 and 4. Next, in section 5 we present a numerical example in which we compare the derived limiting kinetic

models with Monte Carlo simulations for the corresponding individual based model. Finally, in section 6 we provide a specific physical model of a self-propelled nanoparticle swimming in a viscous flow. We present both the individual based model and the corresponding (prelimiting) Fokker–Planck equation.

2. Main results. We start with the Fokker–Planck equation describing random dynamics of an active rod with inertia [4, 11, 36]:

(1) 
$$\partial_{t} f_{\varepsilon} + \frac{1}{\varepsilon} \boldsymbol{v} \cdot \nabla_{\boldsymbol{r}} f_{\varepsilon} + \frac{1}{\varepsilon^{2}} \nabla_{\boldsymbol{v}} \cdot ((\varepsilon \boldsymbol{u} - \boldsymbol{v}) f_{\varepsilon} - D_{\mathrm{tr}} \nabla_{\boldsymbol{v}} f_{\varepsilon}) + \frac{1}{\varepsilon} \omega \partial_{\varphi} f_{\varepsilon} + \frac{1}{\varepsilon^{2}} \partial_{\omega} ((\varepsilon T - \omega) f_{\varepsilon} - D_{\mathrm{rot}} \partial_{\omega} f_{\varepsilon}) = 0.$$

The unknown function  $f_{\varepsilon}(t, \boldsymbol{r}, \boldsymbol{v}, \varphi, \omega)$  is the probability distribution function of the active rod's location  $\boldsymbol{r} \in \Omega \subset \mathbb{R}^2$ , translational velocity  $\boldsymbol{v} \in \mathbb{R}^2$ , orientation angle  $\varphi \in [-\pi, \pi)$ , and angular velocity  $\omega \in \mathbb{R}$ . The given functions  $\boldsymbol{u} = \boldsymbol{u}(\boldsymbol{r}, \varphi)$  and  $T = T(\boldsymbol{r}, \varphi)$  are smooth in  $\Omega \times [-\pi, \pi)$  and  $2\pi$ -periodic in  $\varphi$ . Domain  $\Omega \subset \mathbb{R}^2$  possesses a nonempty smooth boundary. Small positive parameter  $\varepsilon \ll 1$  measures the effect of inertia on dynamics of an active rod.  $D_{\mathrm{tr}}$  and  $D_{\mathrm{rot}}$  are translational and rotational diffusion coefficients, respectively. The unknown function  $f_{\varepsilon}$  is  $2\pi$ -periodic in  $\varphi$ . In addition, the following boundary condition is imposed on  $f_{\varepsilon}$ :

(2) 
$$\mathbf{v} f_{\varepsilon} \cdot \mathbf{n} = \mathbf{v}' f_{\varepsilon}' \cdot (-\mathbf{n}), \mathbf{r} \text{ on } \Gamma.$$

Here  $\Gamma$  is the boundary of  $\Omega$  (a wall of the container),  $\boldsymbol{n}$  is the outward normal, and  $f'_{\varepsilon} = f_{\varepsilon}(t, \boldsymbol{r}, \boldsymbol{v}', \varphi, \omega')$ , where pairs  $(\boldsymbol{v}, \omega)$  and  $(\boldsymbol{v}', \omega')$  represent translational and angular velocities of the active rod before and after a collision with the wall. The relation between the two pairs of velocities is given by

(3) 
$$\begin{bmatrix} v' \\ \omega' \end{bmatrix} = \mathcal{C} \begin{bmatrix} v \\ \omega \end{bmatrix}, \quad \mathcal{C} \in \mathbb{R}^{3 \times 3}, \quad |\det \mathcal{C}| = 1.$$

The specific form of matrix C and the derivation of the kinetic model (1)–(2) from the individual dynamics of an active rod are relegated to section 6.1.

To simplify notations, denote  $\mathcal{X} := (\boldsymbol{r}, \varphi), \, \mathcal{V} := (\boldsymbol{v}, \omega), \, \mathcal{U} := (\boldsymbol{u}, T), \, \text{and}$ 

$$\mathcal{D} := \left[ \begin{array}{ccc} D_{\rm tr} & 0 & 0 \\ 0 & D_{\rm tr} & 0 \\ 0 & 0 & D_{\rm rot} \end{array} \right].$$

In the new notations, the Fokker–Planck equation (1) is

(4) 
$$\partial_t f_{\varepsilon} + \frac{1}{\varepsilon} \mathcal{V} \cdot \nabla_{\mathcal{X}} f_{\varepsilon} + \frac{1}{\varepsilon^2} \nabla_{\mathcal{V}} \cdot ((\varepsilon \mathcal{U} - \mathcal{V}) f_{\varepsilon} - \mathcal{D} \nabla_{\mathcal{V}} f_{\varepsilon}) = 0.$$

Our first main result is the reduction, for small  $\varepsilon$ , of the unknown function  $f_{\varepsilon}(t, \mathcal{X}, \mathcal{V})$  depending on a 7-dimensional variable to the unknown function  $\rho(t, \mathcal{X})$  depending on a 4-dimensional variable. The result is formulated in the following theorem.

Theorem 2.1. Let  $\rho_{\varepsilon}$  be defined by

$$\rho_{\varepsilon}(t,\mathcal{X}) := \int_{\mathbb{R}^3} f_{\varepsilon}(t,\mathcal{X},\mathcal{V}) \,\mathrm{d}\mathcal{V},$$

where  $f_{\varepsilon}$  solves the Fokker-Planck equation (4) with boundary condition (2). Then  $\rho_{\varepsilon}$  converges to  $\rho$  in the distributional sense, as  $\varepsilon \to 0$ , where  $\rho$  satisfies the following limiting equation:

(5) 
$$\partial_t \rho + \nabla_{\mathcal{X}} \cdot (\mathcal{U}\rho) = \nabla_{\mathcal{X}} \cdot \mathcal{D}\nabla_{\mathcal{X}}\rho$$

with the boundary condition

(6) 
$$D_{\text{tr}} \frac{\partial \rho}{\partial \mathbf{n}} = (\mathbf{u} \cdot \mathbf{n}) \rho, \quad \mathbf{r} \ on \ \Gamma, \quad -\pi \le \varphi < \pi.$$

Recall that  $\mathcal{U} = (\boldsymbol{u}, T)$ .

The proof of Theorem 2.1 is given in section 3. This theorem means that the elastic collision boundary condition (2) for  $f_{\varepsilon}$  transforms into the no-flux boundary condition (6) for  $\rho$ . The vanishing inertia limit in the Fokker–Planck equation for spherical particles (no  $\varphi$ ) was considered in [12, 22, 23]. The main difference, besides no  $\varphi$ , is that in [12, 22, 23], u is not given but instead solves the Navier–Stokes equation. In principle, a system with the Navier–Stokes equation is obviously more complicated; on the other hand, the Navier–Stokes equation has an additional dissipation term in the energy relation. Also, the coupling term leads to a certain cancellation in the energy relation (the term  $\int \int \mathcal{U} \cdot (\mathcal{V} - \varepsilon \mathcal{U}) f_{\varepsilon}$  in (15) from section 3). The scaling (that is, how  $\varepsilon$  is introduced in the Fokker–Planck equation) in (4) is similar to [12], but the boundary conditions in [12] are simpler (periodic). In [23] the asymptotic regime of the Fokker–Planck equation is studied for the reflection boundary condition (spherical particles elastically collide with walls) as well, but due to no slip conditions for u (which imply no flow at boundary  $\Gamma$ ), the limiting boundary conditions were not investigated.

In experimental observations, rod-like microswimmers, such as bacteria or bimetallic particles, are more likely to spontaneously turn rather than jump to another position. In other words, random forces along the perimeter of a microswimmer caused by collisions with molecules of the fluid likely result in a significant torque whereas a net force is small. These observations imply that the translational diffusion coefficient is small,  $D_{\rm tr} \ll 1$ . Hence, it is natural to study the limit  $D_{\rm tr} \to 0$ . This limit is singular in the case of active particles; that is, one cannot simply set  $D_{\rm tr}$  to zero in both the Fokker–Planck equation (5) and the no-flux condition (6) in order to obtain the limiting system as  $D_{\rm tr} \to 0$ . This is because active particles tend to accumulate at walls, and in particular they form a boundary layer of the width  $\sim D_{\rm tr}$ . Moreover, from boundary conditions (6) it follows that  $\nabla \rho$  may blow up near boundary  $\Gamma$  in the limit  $D_{\rm tr} \to 0$ ; in this case for stable numerical simulation of (5)–(6) with small  $D_{\rm tr}$  one needs a very fine mesh resulting in high computational complexity of the simulations.

To investigate vanishing translational diffusion  $D_{\rm tr}$  we re-denote the translational diffusion coefficient by symbol  $\mu$  which is used for notations of a small parameter:

$$\mu := D_{\mathrm{tr}}.$$

Then problem (5)–(6) consists of the Fokker–Planck equation:

(7) 
$$\partial_t \rho + \nabla_r \cdot (\boldsymbol{u}\rho) + \partial_{\varphi}(T\rho) = \mu \Delta_r \rho + D_{\text{rot}} \partial_{\varphi}^2 \rho$$

and the boundary condition

(8) 
$$\mu \frac{\partial \rho}{\partial \boldsymbol{n}} = (\boldsymbol{u} \cdot \boldsymbol{n}) \rho, \quad \boldsymbol{r} \text{ on } \Gamma, \quad -\pi \le \varphi < \pi.$$

Our second main result is the derivation of the limit in problem (7)–(8) as  $\mu \to 0$ . The derivation is done by formal multiscale asymptotic expansion; we formulate the result as a conjecture since rigorous justification of the multiscale asymptotic expansions is out of the scope of this work.

CONJECTURE. In the limit  $\mu \to 0$  the probability distribution function  $\rho(t, \mathbf{r}, \varphi)$  has the following representation:

(9) 
$$\rho(t, \mathbf{r}, \varphi) = \psi_{\text{wall}}(t, \mathbf{r}, \varphi) \, \delta_{\Gamma}(\mathbf{r}) + \rho_{\text{bulk}}(t, \mathbf{r}, \varphi).$$

Here  $\delta_{\Gamma}(\mathbf{r})$  is the  $\delta$ -function distribution supported on  $\Gamma = \{\gamma(s) : 0 \leq s \leq L\}$  (s is the arc-length parameter of curve  $\Gamma$ ), and probability distribution functions  $\rho_{bulk}$  and  $\psi_{wall}$  solve the following system:

$$\begin{array}{l} \partial_{t}\rho_{\mathrm{bulk}} + \nabla_{\boldsymbol{r}} \cdot (\boldsymbol{u}\rho_{\mathrm{bulk}}) + \partial_{\varphi}(T\rho_{\mathrm{bulk}}) = D_{\mathrm{rot}}\partial_{\varphi}^{2}\rho_{\mathrm{bulk}} + \sum_{i=1,2} \chi_{i} \, \delta_{\Gamma}(\boldsymbol{r})\delta(\varphi - \varphi_{i}), \\ \boldsymbol{r} \in \Omega, \quad -\pi \leq \varphi < \pi, \\ \partial_{t}\psi_{\mathrm{wall}} + \partial_{s}((\boldsymbol{u} \cdot \boldsymbol{\tau})\psi_{\mathrm{wall}}) + \partial_{\varphi}(T\psi_{\mathrm{wall}}) = D_{\mathrm{rot}}\partial_{\varphi}^{2}\psi_{\mathrm{wall}} + (\boldsymbol{u} \cdot \boldsymbol{n})\rho_{\mathrm{bulk}}, \\ \boldsymbol{r} \in \Gamma, \, s \in [0, L], \, \varphi \in (\varphi_{1}, \varphi_{2}), \\ \rho_{\mathrm{bulk}} = 0, \quad \boldsymbol{r} \in \Gamma, \quad \varphi \notin [\varphi_{1}, \varphi_{2}], \quad \rho_{\mathrm{bulk}} \, \mathrm{is} \, 2\pi - \mathrm{periodic} \, \mathrm{in} \, \varphi \, \mathrm{for} \, \mathrm{all} \, \boldsymbol{r} \in \Omega, \\ \psi_{\mathrm{wall}} = 0, \quad s \in [0, L], \quad \varphi \in \{\varphi_{1}, \varphi_{2}\}, \\ \chi_{i}(s, \varphi) := (-1)^{i} (T\psi_{\mathrm{wall}} - D_{\mathrm{rot}}\partial_{\varphi}\psi_{\mathrm{wall}}), \quad i = 1, 2. \end{array}$$

Here  $\tau$  denotes the tangential vector of  $\Gamma$ , and angles  $\varphi_1(s)$  and  $\varphi_2(s)$  are introduced such that

$$\mathbf{u} \cdot \mathbf{n} > 0$$
 for  $\varphi \in (\varphi_1(s), \varphi_2(s))$  and  $\mathbf{u} \cdot \mathbf{n} \leq 0$  otherwise.

Representation (9) means that the total probability distribution function  $\rho$  consists of the regular part,  $\rho_{\text{bulk}}$ , describing distribution of particles in the bulk, and the singular part,  $\psi_{\text{wall}} \delta_{\Gamma}$ , describing distribution of particles accumulated at wall. Derivation of system (10) is presented in section 4. We also provide a numerical example in section 5 in which we test the derived kinetic approaches (7)–(8) and (10) with results of Monte Carlo simulations for the corresponding individual based model.

Our results, Theorem 2.1 and the conjecture, are formulated for the two-dimensional (2D) case. Active rod-like microswimmers in two dimensions,  $\Omega \subset \mathbb{R}^2$ , have been extensively studied both experimentally and theoretically; see, e.g., [6, 24, 28, 31, 37, 38, 39, 43, 44]. Our results are also applicable for three-dimensional domains,  $\Omega \subset \mathbb{R}^3$ . In this case the orientation of an active rod is described by two angles, azimuthal angle  $0 \le \varphi < 2\pi$ , and polar angle  $0 \le \theta \le \pi$ , and derivatives in angle for the 2D model in (1) and (7) are to be replaced by spherical gradient  $\nabla_{\varphi,\theta}$  and spherical Laplacian  $\Delta_{\varphi,\theta}$ . For example, in the three-dimensional case, the Fokker-Planck equation (7) is written as follows:

$$\partial_t \rho + \nabla_{\mathbf{r}} \cdot (\mathbf{u}\rho) + \nabla_{\varphi,\theta} \cdot (T\rho) = \mu \Delta_{\mathbf{r}} \rho + D_{\text{rot}} \Delta_{\varphi,\theta} \rho.$$

For the definition of differential operators  $\nabla_{\varphi,\theta}$  and  $\Delta_{\varphi,\theta}$  we refer, for example, to [13, section 2]. The main difference in formulation of the conjecture about the limit  $\mu \to 0$  in three dimensions, compared to two dimensions, is that the angle pair  $\{\varphi_1, \varphi_2\}$  is to be replaced by the set  $\{(\varphi, \theta) : \mathbf{u} \cdot \mathbf{n} = 0\}$ .

## 3. Vanishing inertia limit in the Fokker-Planck equation.

*Proof of Theorem* 2.1. In this section we take  $D_{\rm tr}=D_{\rm rot}=1$  for the sake of simplicity. To consider the limit  $\varepsilon\to 0$ , introduce the mean flux (or the mean velocity) and the "kinetic pressure":

$$J_{\varepsilon}(t,\mathcal{X}):=\frac{1}{\varepsilon}\int_{\mathbb{R}^3}\mathcal{V}f_{\varepsilon}\,\mathrm{d}\mathcal{V}\quad\text{and}\quad \mathbb{P}_{\varepsilon}(t,\mathcal{X}):=\int_{\mathbb{R}^3}\mathcal{V}\otimes\mathcal{V}f_{\varepsilon}\,\mathrm{d}\mathcal{V}.$$

By integration of (4) with respect to  $d\mathcal{V}$  and  $\varepsilon \mathcal{V} d\mathcal{V}$  one obtains the system for  $\rho_{\varepsilon}$  and  $J_{\varepsilon}$ :

(11) 
$$\partial_t \rho_{\varepsilon} + \nabla_{\mathcal{X}} \cdot J_{\varepsilon} = 0,$$

(12) 
$$\varepsilon^2 \partial_t J_{\varepsilon} + \nabla_{\mathcal{X}} \cdot \mathbb{P}_{\varepsilon} = \rho_{\varepsilon} \mathcal{U} - J_{\varepsilon}.$$

By using arguments similar to [12], we will show that the limit of (12) is  $J = \rho \mathcal{U} - \nabla_{\mathcal{X}} \rho$ . Substitution of this formula for J into the limiting version of (11) (that is, (11) without subindexes  $\varepsilon$ ) then gives

$$\partial_t \rho + \nabla_{\mathcal{X}} \cdot (\mathcal{U}\rho) = \Delta_{\mathcal{X}} \rho.$$

The main question is how to find the boundary condition for  $\rho$ . Note that from collision boundary condition (2) it follows that active rods cannot leave domain  $\Omega$ , that is, there is no flux through the boundary  $\Gamma$ :

$$\hat{J}_{\varepsilon} \cdot \boldsymbol{n} = 0 \text{ on } \Gamma,$$

where  $\hat{J}_{\varepsilon} = (J_1, J_2)$  (no  $J_3$ , corresponding to the flux of orientations  $\varphi$ ). The main purpose of this section is to prove that this relation is preserved in the limit  $\varepsilon \to 0$ , which, taking into account the formula for the limiting flux  $J = \rho \mathcal{U} - \nabla_{\mathcal{X}} \rho$ , is equivalent to

(13) 
$$\frac{\partial \rho}{\partial \boldsymbol{n}} = (\boldsymbol{u} \cdot \boldsymbol{n})\rho.$$

In order to prove Theorem 2.1 we will use two auxiliary propositions. In Proposition 1, the energy estimate is established. This estimate leads to a priori bounds needed to obtain that the family  $\{f_{\varepsilon}\}_{\varepsilon}$  has a limit as  $\varepsilon \to 0$  (Proposition 2).

We first introduce the following notations:

$$\mathcal{E}_{\varepsilon}(t) := \int_{\mathbb{R}^{2} \times \mathbb{R}} \int_{\Omega \times (-\pi, \pi)} \left\{ \frac{\boldsymbol{v}^{2}}{2} + \frac{\omega^{2}}{2} + \ln f_{\varepsilon} \right\} f_{\varepsilon} \, d\mathcal{X} d\mathcal{V},$$
$$d_{\varepsilon}(t, \mathcal{X}, \mathcal{V}) := \left( (\mathcal{V} - \varepsilon \mathcal{U}) + \nabla_{\mathcal{V}}(\ln f_{\varepsilon}) \right) \sqrt{f_{\varepsilon}}.$$

Recall that  $\mathcal{X} = (\boldsymbol{r}, \varphi) \in \Omega \times [-\pi, \pi)$  and  $\mathcal{V} = (\boldsymbol{v}, \omega) \in \mathbb{R}^2_{\boldsymbol{v}} \times \mathbb{R}_{\omega} = \mathbb{R}^3$ .

PROPOSITION 1. There exists a constant C, independent of  $\varepsilon$ , such that the following estimate (the entropy inequality) holds:

(14) 
$$\frac{\mathrm{d}}{\mathrm{d}t} \mathcal{E}_{\varepsilon}(t) + \frac{1}{2\varepsilon^2} \int_{\mathbb{R}^3} \int_{\Omega \times (-\pi, \pi)} |d_{\varepsilon}|^2 \, \mathrm{d}\mathcal{X} \, \mathrm{d}\mathcal{V} < C.$$

*Proof.* Multiplication of (4) by

$$\frac{\boldsymbol{v}^2}{2} + \frac{\omega^2}{2} + \ln f_{\varepsilon}$$

and integration with respect to both  $\mathcal{X}$  and  $\mathcal{V}$  gives

$$\frac{\mathrm{d}}{\mathrm{d}t} \left[ \int_{\mathbb{R}^{3}} \int_{\Omega \times (-\pi,\pi)} \left\{ \frac{\mathbf{v}^{2}}{2} + \frac{\omega^{2}}{2} + \ln f_{\varepsilon} \right\} f_{\varepsilon} \, \mathrm{d}\mathcal{X} \, \mathrm{d}\mathcal{V} \right] = 
= -\frac{1}{\varepsilon} \int_{\mathbb{R}^{3}} \int_{-\pi}^{\pi} \int_{\Gamma} \left\{ \frac{\mathbf{v}^{2}}{2} + \frac{\omega^{2}}{2} + \ln f_{\varepsilon} \right\} (\mathbf{v} \cdot \mathbf{n}) f_{\varepsilon} \, \mathrm{d}s_{\mathbf{r}} \, \mathrm{d}\varphi \, \mathrm{d}\mathcal{V} 
- \frac{1}{\varepsilon^{2}} \int_{\mathbb{R}^{3}} \int_{\Omega \times (-\pi,\pi)} \left| (\mathcal{V} - \varepsilon \mathcal{U}) + \nabla_{\mathcal{V}} (\ln f_{\varepsilon}) \right|^{2} f_{\varepsilon} \, \mathrm{d}\mathcal{X} \, \mathrm{d}\mathcal{V} 
- \frac{1}{\varepsilon} \int_{\mathbb{R}^{3}} \int_{\Omega \times (-\pi,\pi)} \mathcal{U} \cdot (\mathcal{V} - \varepsilon \mathcal{U}) f_{\varepsilon} \, \mathrm{d}\mathcal{X} \, \mathrm{d}\mathcal{V}.$$
(15)

Next we compute the boundary term in the right-hand side of (15) (the one with the integral over  $\Gamma$ ). To this end, we use boundary condition (2). For each  $r \in \Gamma$  and  $-\pi \leq \varphi < \pi$  denote

(16) 
$$S_{\sigma>0} := \{ (\boldsymbol{v}, \omega) : \sigma > 0 \} \text{ and } S_{\sigma<0} := \{ (\boldsymbol{v}, \omega) : \sigma < 0 \},$$

where  $\sigma = \sigma(\mathbf{r}, \mathbf{v}, \varphi, \omega)$  is given by (53) in section 6.1. The introduced sets  $S_{\sigma>0}$  and  $S_{\sigma<0}$  can be understood as sets of configurations (velocities) of an active rod before and after a collision, respectively, at the given location of the boundary  $\mathbf{r} \in \Gamma$  and the given orientation  $\varphi \in [-\pi, \pi)$ . Then the boundary integral can be written as follows for each  $\mathbf{r} \in \Gamma$  and  $-\pi \leq \varphi < \pi$ :

$$\int_{\mathbb{R}^3} \left\{ \frac{\boldsymbol{v}^2}{2} + \frac{\omega^2}{2} + \ln f_{\varepsilon} \right\} (\boldsymbol{v} \cdot \boldsymbol{n}) f_{\varepsilon} \, d\mathcal{V} 
= \int_{S_{\sigma<0}} \left\{ \frac{\boldsymbol{v}^2}{2} + \frac{\omega^2}{2} + \ln f_{\varepsilon} \right\} (\boldsymbol{v} \cdot \boldsymbol{n}) f_{\varepsilon} \, d\mathcal{V} + \int_{S_{\sigma>0}} \left\{ \frac{\boldsymbol{v}^2}{2} + \frac{\omega^2}{2} + \ln f_{\varepsilon} \right\} (\boldsymbol{v} \cdot \boldsymbol{n}) f_{\varepsilon} \, d\mathcal{V}.$$

We claim that the two integrals in the right-hand side of the equality above cancel each other. To verify this, one needs to make the substitution in the first integral  $\mathcal{V}' = \mathcal{C}\mathcal{V}$  with  $\mathcal{C}$  from (3) and to use boundary condition (2), the conservation of energy during a collision (see, e.g., (52)), and  $d\mathcal{V}' = d\mathcal{V}$  which follows from  $|\det \mathcal{C}| = 1$  (see (3)). Hence, the boundary term in the right-hand side of (15) vanishes.

Note that in the same manner one can show the conservation of total  $f_{\varepsilon}$ :

$$\frac{\mathrm{d}}{\mathrm{d}t} \left[ \int_{\mathbb{R}^3} \int_{\Omega \times (-\pi,\pi)} f_{\varepsilon} \, \mathrm{d}\mathcal{X} \mathrm{d}\mathcal{V} \right] = 0.$$

Indeed, by using (4) and integration by parts it follows that

$$\frac{\mathrm{d}}{\mathrm{d}t} \left[ \int_{\mathbb{R}^3} \int_{\Omega \times (-\pi,\pi)} f_{\varepsilon} \, \mathrm{d}\mathcal{X} \, \mathrm{d}\mathcal{V} \right] = -\frac{1}{\varepsilon} \int_{\mathbb{R}^3} \int_{-\pi}^{\pi} \int_{\Gamma} (\boldsymbol{v} \cdot \boldsymbol{n}) f_{\varepsilon} \, \mathrm{d}s_{\boldsymbol{r}} \, \mathrm{d}\varphi \, \mathrm{d}\mathcal{V},$$

and one can show that the right-hand side vanishes following the same arguments as for the boundary term in (15)

Finally, the last term in the right-hand side of (15) is estimated as follows:

$$-\frac{1}{\varepsilon} \int_{\mathbb{R}^{3}} \int_{\Omega \times (-\pi,\pi)} \mathcal{U} \cdot (\mathcal{V} - \varepsilon \mathcal{U}) f_{\varepsilon} \, d\mathcal{X} d\mathcal{V} 
= -\frac{1}{\varepsilon} \int_{\mathbb{R}^{3}} \int_{\Omega \times (-\pi,\pi)} \mathcal{U} \cdot ((\mathcal{V} - \varepsilon \mathcal{U}) + \nabla_{\mathcal{V}}(\ln f_{\varepsilon})) f_{\varepsilon} \, d\mathcal{X} d\mathcal{V} 
(17) \qquad \leq C + \frac{1}{2\varepsilon^{2}} \int_{\mathbb{R}^{3}} \int_{\Omega \times (-\pi,\pi)} |d_{\varepsilon}|^{2} \, d\mathcal{X} d\mathcal{V}.$$

Thus, we obtained (14), and the proposition is proved.

In the standard manner (see, e.g., [12]) the entropy estimate (14) implies the following bounds:

$$\begin{split} f_{\varepsilon}\left(1+\frac{\boldsymbol{v}^2}{2}+\frac{\omega^2}{2}+|\ln f_{\varepsilon}|\right) & \text{ is bounded in } \quad L^{\infty}(0,T;L^1(\Omega\times(-\pi,\pi)\times\mathbb{R}^3)),\\ \varepsilon^{-1}d_{\varepsilon} & \text{ is bounded in } \quad L^2(0,T;L^2(\Omega\times(-\pi,\pi)\times\mathbb{R}^3)),\\ \rho_{\varepsilon} & \text{ is bounded in } \quad L^{\infty}(0,T;L^1(\Omega\times(-\pi,\pi))),\\ J_{\varepsilon} & \text{ and } J_{\varepsilon}-\rho_{\varepsilon}\mathcal{U} & \text{ are bounded in } \quad L^2(0,T;L^1(\Omega\times(-\pi,\pi))). \end{split}$$

The proof of the following proposition is also standard and can be found in [12].

PROPOSITION 2. There exist such  $\rho$  and J that the following convergences hold as  $\varepsilon \to 0$  in the distributional sense:

(18) 
$$\rho_{\varepsilon} \rightharpoonup \rho, \ J_{\varepsilon} \rightharpoonup J, \ \mathbb{P}_{\varepsilon} \rightharpoonup \rho \mathbb{I}.$$

Here  $\mathbb{I}$  is identity matrix.

Now we are in position to complete the proof of Theorem 2.1.

Back to the proof of Theorem 2.1. By multiplication of (4) by a scalar test functions  $\psi(t, \mathcal{X}, \mathcal{V})$  with a finite support in 0 < t < T,  $\mathcal{X} \in \Omega \times (-\pi, \pi)$  and  $\mathcal{V} \in \mathbb{R}^3$ , integration with respect to t,  $\mathcal{X}$  and  $\mathcal{V}$ , as well as integration by parts, one obtains the following equality:

$$\int_{0}^{T} \int_{\mathbb{R}^{3}} \int_{\Omega \times (-\pi,\pi)} f_{\varepsilon} \left\{ \partial_{t} \psi + \frac{1}{\varepsilon} \mathcal{V} \cdot \nabla_{\mathcal{X}} \psi + \frac{1}{\varepsilon^{2}} (\varepsilon \mathcal{U} - \mathcal{V}) \cdot \nabla_{\mathcal{V}} \psi + \frac{1}{\varepsilon^{2}} \Delta_{\mathcal{V}} \psi \right\} d\mathcal{X} d\mathcal{V} dt 
(19) \qquad \qquad -\frac{1}{\varepsilon} \int_{0}^{T} \int_{\Gamma} \int_{-\pi}^{\pi} \int_{S_{\kappa} > 0} (\boldsymbol{v} \cdot \boldsymbol{n}) f_{\varepsilon} (\psi - \psi') d\mathcal{V} d\varphi ds_{\boldsymbol{r}} dt = 0,$$

where  $\psi' = \psi(t, \mathcal{X}, \mathcal{V}')$  with  $\mathcal{V}' = \mathcal{C}\mathcal{V}$ , and matrix  $\mathcal{C}$  and set  $S_{\sigma>0}$  are defined by (55) and (16), respectively. Equality (19) can be understood as the weak formulation of the problem (4) with boundary condition (2).

Next, take a test function in (19) which is independent of  $\mathcal{V}$ :  $\psi := g(t, \mathcal{X})$  (for the sake of clarity, choose different symbol for the test function here: g instead of  $\psi$ ). Formally, such a test function is not admissible since it does not have a finite support in  $\mathcal{V}$ . On the other hand, one can use truncations  $g(t, \mathcal{X}) \cdot \mathbb{1}_{|\mathcal{V}| < R}(\mathcal{V})$  as test functions and pass to the limit  $R \to \infty$  to obtain (19) for  $\psi = g(t, \mathcal{X})$ . By integrating in  $\mathcal{V}$  we obtain

$$\int_0^T \int_{\Omega \times (-\pi,\pi)} \rho_{\varepsilon} \partial_t g + J_{\varepsilon} \cdot \nabla_{\mathcal{X}} g \, d\mathcal{X} dt = 0.$$

Note that the boundary term in (19) vanishes for test functions independent from  $\mathcal{V}$ . By passing to the limit  $\varepsilon \to 0$  we obtain

(20) 
$$\int_{0}^{T} \int_{\Omega \times (-\pi, \pi)} \rho \partial_{t} g + J \cdot \nabla_{\mathcal{X}} g \, d\mathcal{X} dt = 0.$$

Take the test function of the form  $\psi := \varepsilon v_i h_i(t, \mathcal{X})$  for i = 1, 2:

(21) 
$$\int_{0}^{T} \int_{\Omega \times (-\pi,\pi)} \varepsilon^{2} J_{\varepsilon}^{i} \partial_{t} h_{i} + \mathbb{P}_{\varepsilon}^{ij} \partial_{\mathcal{X}_{j}} h_{i} + (\rho_{\varepsilon} \mathcal{U}^{i} - J_{\varepsilon}^{i}) h_{i} \, d\mathcal{X} dt$$
$$-2 \int_{0}^{T} \int_{\mathbb{R}} \int_{-\pi}^{\pi} \int_{\Gamma} \int_{S_{\sigma} > 0} \sigma(\boldsymbol{v} \cdot \boldsymbol{n}) f_{\varepsilon} h_{i} n_{i} \, d\boldsymbol{v} ds_{x} d\varphi d\omega dt = 0.$$

Here both the super- and subindex i stand for the coordinate number. Consider  $\mathbf{h} = \{h_i\}_{i=1}^3$  so that  $\mathbf{h} \cdot \mathbf{n} = h_1 n_1 + h_2 n_2 = 0$  for all  $-\pi \leq \varphi < \pi$  and  $h_3(t, \mathcal{X})$  is arbitrary. The test function  $\psi$  corresponding to  $h_3(t, \mathcal{X})$  is  $\psi = \omega h_3(t, \mathcal{X})$ , and in this case equality (21) holds for i = 3 with no second (boundary) term. Then taking the sum with respect to i in (21) leads to that the boundary term in (21) vanishes, so that the following equality holds:

$$\int_0^T \int_{\Omega \times (-\pi,\pi)} \varepsilon^2 J_{\varepsilon} \cdot \partial_t \boldsymbol{h} + \mathbb{P}_{\varepsilon} : \nabla_{\mathcal{X}} \boldsymbol{h} + (\rho_{\varepsilon} \mathcal{U} - J_{\varepsilon}) \cdot \boldsymbol{h} \, d\mathcal{X} dt = 0.$$

Passing to the limit  $\varepsilon \to 0$  and using Proposition 2 we get

(22) 
$$\int_0^T \int_{\Omega \times (-\pi, \pi)} \rho \mathbb{I} : \nabla_{\mathcal{X}} \boldsymbol{h} + (\rho \mathcal{U} - J) \cdot \boldsymbol{h} \, d\mathcal{X} dt = 0.$$

This equality gives us the following relation for J:

(23) 
$$\int_0^T \int_{\Omega \times (-\pi,\pi)} J \cdot \boldsymbol{h} \, d\mathcal{X} dt = \int_0^T \int_{\Omega \times (-\pi,\pi)} \rho \mathbb{I} : \nabla_{\mathcal{X}} \boldsymbol{h} + \rho \mathcal{U} \cdot \boldsymbol{h} \, d\mathcal{X} dt$$

for all  $\boldsymbol{h}$  such that  $h_1 n_1 + h_2 n_2|_{\Gamma} = 0$  for all  $-\pi \leq \varphi < \pi$ . Finally, take any  $g(t, \mathcal{X})$  in (20) such that  $\frac{\partial g}{\partial \boldsymbol{n}}|_{\Gamma} = 0$  for all  $-\pi \leq \varphi < \pi$  and  $\boldsymbol{h} := \nabla_{\mathcal{X}} g$  in (23) to express  $\int_0^T \int_{\Omega \times (-\pi,\pi)} J \cdot \nabla_{\mathcal{X}} g \, \mathrm{d}\mathcal{X} \, \mathrm{d}t$  in (20). We obtain the following weak formulation for the equation for  $\rho$ :

(24) 
$$\int_{0}^{T} \int_{\Omega \times (-\pi, \pi)} \left\{ \rho \partial_{t} g + \rho \mathcal{U} \cdot \nabla_{\mathcal{X}} g + \rho \mathbb{I} : \nabla_{\mathcal{X}}^{2} g \right\} d\mathcal{X} dt = 0$$

for all g such that  $\frac{\partial g}{\partial \mathbf{n}}|_{\Gamma} = 0$  for all  $-\pi \leq \varphi < \pi$ . By integrating by parts and using condition  $\frac{\partial g}{\partial \mathbf{n}}|_{\Gamma} = 0$ , (24) leads to

(25) 
$$\int_{0}^{T} \int_{\Omega \times (-\pi,\pi)} g \left\{ \partial_{t} \rho + \nabla_{\mathcal{X}} \cdot (\rho \mathcal{U}) - \Delta_{\mathcal{X}} \rho \right\} d\mathcal{X} dt + \int_{0}^{T} \int_{-\pi}^{\pi} \int_{\Gamma} g \left\{ -\frac{\partial \rho}{\partial \boldsymbol{n}} + (\boldsymbol{u} \cdot \boldsymbol{n}) \rho \right\} ds_{\boldsymbol{r}} d\varphi dt = 0.$$

Varying g on  $\Gamma$  we get our final result which is the no-flux boundary condition (13):

$$\frac{\partial \rho}{\partial \boldsymbol{n}} = (\boldsymbol{u} \cdot \boldsymbol{n})\rho$$

for all  $-\pi \leq \varphi < \pi$ .

Thus, the proof of Theorem 2.1 is complete.

Remark 1. Throughout the proof of Theorem 2.1, functions  $f_{\varepsilon}$  and  $\rho$  are assumed to be weak solutions for problems (1)–(2) and (7)–(8), respectively. Specifically,

$$f_{\varepsilon} \in L^{\infty}((0,\infty); L^{1}(\Omega \times (-\pi,\pi) \times \mathbb{R}^{3}_{\mathcal{V}})), \quad \rho \in L^{\infty}((0,\infty); L^{1}(\Omega \times (-\pi,\pi))),$$
$$(\boldsymbol{v} \cdot \boldsymbol{n}) f_{\varepsilon} \in L^{1}((0,\infty) \times \Gamma \times (-\pi,\pi) \times \mathbb{R}^{3}_{\mathcal{V}})$$

such that  $f_{\varepsilon}$  and  $\rho$  satisfy weak formulations (19) and (24), respectively. If functions  $f_{\varepsilon}$  and  $\rho$  are sufficiently smooth, integration by parts in weak formulations recovers the respective boundary conditions (2) and (6).

4. Boundary layer equation at wall in vanishing translational diffusion limit: derivation of (10). To describe the behavior of  $\rho$  near the wall, one needs to consider the limiting behavior of  $\rho$  inside the "band"  $\Omega^* := \{ r \in \Omega : \operatorname{dist}(r, \Gamma) < c \}$ , where c is small but independent of  $\mu$ . Here we choose c > 0 such that  $c < \kappa_{\max}^{-1}$ , where  $\kappa_{\max}$  is the maximum curvature along  $\Gamma$ . If  $\Gamma$  is a straight line or a segment, then curvature  $\kappa$  is zero, and c is an arbitrary number independent of  $\mu$ .

We introduce a new coordinate system in band  $\Omega^*$ , related to parametrization of wall  $\Gamma = \partial \Omega$ . Namely, let  $\Gamma = \{ \gamma(s) : 0 \le s \le L \}$  be the natural parametrization of the wall  $\Gamma$  (in other words, s is the arc length parameter) and n(s),  $\tau(s)$  be outward normal and tangential vectors at  $\gamma(s) \in \Gamma$ , respectively. For every  $r \in \Omega^*$ , we define

(26) 
$$\mathbf{r} = \mathbf{r}(r,s) = \mathbf{\gamma}(s) - r\mathbf{n}(s),$$

where  $r = \operatorname{dist}(\mathbf{r}, \Gamma)$  and  $\gamma(s)$  is the "projection" of  $\mathbf{r}$  onto  $\Gamma$ .

In this new coordinate system we introduce the two-scale ansatz for unknown function  $\rho$ :

(27) 
$$\rho = \rho_w + \rho_b = \sum_{k=-1}^{\infty} \mu^k \rho_w^{(k)} \left( t, \mu^{-1} r, s, \varphi \right) + \sum_{k=0}^{\infty} \mu^k \rho_b^{(k)} (t, r, s, \varphi).$$

Here subindexes "w" and "b" stand for "wall" and "bulk," respectively. Variable z denotes below the second argument of  $\rho_w^{(k)}$ , the kth wall (boundary layer) coefficient, i.e.,  $z = \mu^{-1}r$  in (27). We assume that functions  $\{\rho_w^{(k)}(t,z,s,\varphi)\}_k$  vanish with all derivatives in z as  $z \to \infty$ . In what follows, we focus on the first three terms of two-scale expansion (27) or, in other words, on terms of order  $\mu^{-1}$  and  $\mu^0$ :

(28) 
$$\rho = \mu^{-1} \rho_w^{(-1)}(t, \mu^{-1} r, s, \varphi) + \rho_w^{(0)}(t, \mu^{-1} r, s, \varphi) + \rho_h^{(0)}(t, r, s, \varphi) + O(\mu).$$

The representations (28) and (9) are related via the following equalities:

(29) 
$$\psi_{\text{wall}}(t, \boldsymbol{r}, \varphi) = \int_0^{+\infty} \rho_w^{(-1)}(t, z, s, \varphi) \, \mathrm{d}z \text{ and } \rho_{\text{bulk}}(t, \boldsymbol{r}, \varphi) = \rho_b^{(0)}(t, r, s, \varphi).$$

Next, we rewrite the Fokker-Planck equation (7) in the coordinate system (r, s). To this end, we introduce the inverse substitution functions R(r) and S(r):

$$egin{array}{ll} r = R(m{r}) &\Leftrightarrow & R(m{\gamma}(s) - rm{n}(s)) = r, \\ s = S(m{r}) &\Leftrightarrow & S(m{\gamma}(s) - rm{n}(s)) = s. \end{array}$$

Using the chain rule and the 2D Frenet–Serret relation for the normal vector  $\mathbf{n}'(s) = -\kappa(s)\boldsymbol{\tau}(s)$  where  $\kappa(s)$  is the curvature of  $\Gamma$  at  $\mathbf{r} = \boldsymbol{\gamma}(s)$ , one obtains

(30) 
$$\nabla_{\mathbf{r}} R = -\mathbf{n} \quad \text{and} \quad \nabla_{\mathbf{r}} S = (1 - \kappa r)^{-1} \boldsymbol{\tau}.$$

To compute  $\nabla_{\boldsymbol{r}}\rho$ ,  $\Delta_{\boldsymbol{r}}\rho$ , and  $\nabla_{\boldsymbol{r}}\cdot\boldsymbol{u}$  one can use (30) and both 2D Frenet–Serret relations,  $\boldsymbol{n}'(s) = -\kappa(s)\boldsymbol{\tau}(s)$  and  $\boldsymbol{\tau}'(s) = \kappa(s)\boldsymbol{n}(s)$ :

$$\nabla_{\boldsymbol{r}}\rho = -\partial_{r}\rho\,\boldsymbol{n} + \frac{\partial_{s}\rho}{1 - \kappa r}\,\boldsymbol{\tau},$$

$$\Delta_{\boldsymbol{r}}\rho = \partial_{r}^{2}\rho - \frac{\kappa\partial_{r}\rho}{1 - \kappa r} + \frac{r(\partial_{s}\kappa)(\partial_{s}\rho)}{(1 - \kappa r)^{3}} + \frac{\partial_{s}^{2}\rho}{(1 - \kappa r)^{2}},$$

$$\nabla_{\boldsymbol{r}} \cdot \boldsymbol{u} = -\partial_{r}\boldsymbol{u}_{n} + \frac{\partial_{s}\boldsymbol{u}_{\tau}}{1 - \kappa r} + \frac{\kappa\boldsymbol{u}_{n}}{1 - \kappa r}.$$

Here  $u_n = \boldsymbol{u} \cdot \boldsymbol{n}$  and  $u_{\tau} = \boldsymbol{u} \cdot \boldsymbol{\tau}$ .

Then the original problem (7)–(8) converts into

$$(31) \qquad \partial_t \rho - u_n \partial_r \rho + \frac{u_\tau \partial_s \rho}{1 - \kappa r} + \left( -\partial_r u_n + \frac{\partial_s u_\tau}{1 - \kappa r} + \frac{\kappa u_n}{1 - \kappa r} \right) \rho + \partial_\varphi (T \rho)$$

$$= \mu \left( \partial_r^2 \rho - \frac{\kappa \partial_r \rho}{1 - \kappa r} + \frac{r(\partial_s \kappa)(\partial_s \rho)}{(1 - \kappa r)^3} + \frac{\partial_s^2 \rho}{(1 - \kappa r)^2} \right) + D_{\text{rot}} \partial_\varphi^2 \rho$$

with boundary conditions

(32) 
$$\mu \frac{\partial \rho}{\partial r} = -u_{\rm n} \rho \text{ if } r = 0.$$

When substituting representation (28) into (31), we will treat the second term in the left-hand side as follows:

$$u_{\rm n}\partial_r \rho = \left(u_{\rm n}^{(0)} + (z\mu)\,u_{\rm n}^{(1)} + \frac{1}{2}(z\mu)^2 u_{\rm n}^{(2)} + \cdots\right)\partial_r \rho_w + u_{\rm n}(r,s)\,\partial_r \rho_b,$$

where  $u_{\rm n}^{(k)}=1/k!\,\partial_r^k u_{\rm n}|_{r=0}$ . Note that  $u_{\rm n}^{(k)}$  is a function of  $\varphi$  and s for each  $k=1,2,\ldots$ 

At the order  $\mu^{-2}$  in (31) one has the following equality:

(33) 
$$u_{\rm n}^{(0)} \partial_z \rho_w^{(-1)} + \partial_z^2 \rho_w^{(-1)} = 0.$$

The lowest order in the boundary conditions (8) is  $\mu^{-1}$ , and the corresponding equality is

(34) 
$$u_{\mathbf{n}}^{(0)}\rho_{w}^{(-1)} + \partial_{z}\rho_{w}^{(-1)} = 0, \quad z = 0.$$

Combining (33) and (34) we obtain a formula for  $\rho_w^{(-1)}$ :

$$\rho_w^{(-1)}(t,z,s,\varphi) = \left\{ \begin{array}{cc} B(t,s,\varphi)e^{-u_{\rm n}^{(0)}z}, & u_{\rm n}^{(0)} < 0, \\ 0, & u_{\rm n}^{(0)} \geq 0. \end{array} \right.$$

At order  $\mu^{-1}$ , the Fokker–Planck equation (31) has the form

$$u_{\mathbf{n}}^{(0)} \partial_{z} \rho_{w}^{(0)} + \partial_{z}^{2} \rho_{w}^{(0)} = \partial_{t} \left( B e^{-u_{\mathbf{n}}^{(0)} z} \right) - u_{\mathbf{n}}^{(0)} B e^{-u_{\mathbf{n}}^{(0)} z} \left( -z u_{\mathbf{n}}^{(1)} + \kappa \right) + u_{\tau}^{(0)} \partial_{s} \left( B e^{-u_{\mathbf{n}}^{(0)} z} \right)$$

$$- \left( u_{\mathbf{n}}^{(1)} - \partial_{s} u_{\tau}^{(0)} - \kappa u_{\mathbf{n}}^{(0)} \right) B e^{-u_{\mathbf{n}}^{(0)} z}$$

$$+ \partial_{\varphi} \left( T B e^{-u_{\mathbf{n}}^{(0)} z} \right) - D_{\mathbf{rot}} \partial_{\varphi}^{2} \left( B e^{-u_{\mathbf{n}}^{(0)} z} \right).$$

$$(35)$$

Boundary conditions at the order  $\mu^0$  look as follows:

$$u_{\rm n}^{(0)}\rho_w^{(0)} + \partial_z \rho_w^{(0)} = -u_{\rm n}^{(0)}\rho_b^{(0)}$$
 for  $z = 0$ .

Consider  $u_{\rm n}^{(0)}>0$ . After integration (35) with respect to z from 0 to  $\infty$  and simplifications one obtains an equation for  $\psi_{\rm wall}=\int_0^\infty \rho_w^{(-1)}\,{\rm d}z=B/u_{\rm n}^{(0)}$ :

(36) 
$$u_{\rm n}^{(0)} \rho_b^{(0)} = \partial_t \psi_{\rm wall} + \partial_s (u_{\tau}^{(0)} \psi_{\rm wall}) + \partial_\varphi (T \psi_{\rm wall}) - D_{\rm rot} \partial_\varphi^2 \psi_{\rm wall}.$$

Equation (36) is a conservation law for the distribution of active rods  $\psi_{\text{wall}}$  accumulated at the wall; these active rods reorient and move along the wall in the tangential

direction. Term  $u_n^{(0)} \rho_b^{(0)}$  in the left-hand side of (36) accounts for particles coming from the bulk. If the divergence-free condition is imposed,  $\nabla_{\mathbf{r}} \cdot u = 0$ , which for r = 0 has the form  $u_n^{(1)} - \partial_s u_\tau^{(0)} - \kappa u_n^{(0)} = 0$ , then (36) can be rewritten in the form

$$u_{\rm n}^{(0)}\rho_b^{(0)} = \partial_t \psi_{\rm wall} + \left(u_{\rm n}^{(1)} - \kappa u_{\rm n}^{(0)}\right)\psi_{\rm wall} + u_{\tau}^{(0)}\partial_s \psi_{\rm wall} + \partial_{\varphi}\left(T\psi_{\rm wall}\right) - D_{\rm rot}\partial_{\varphi}^2\psi_{\rm wall}.$$

If 
$$u_n^{(0)} \le 0$$
, then  $\psi_{\text{wall}} = 0$  and  $\rho_b^{(0)}|_{r=0} = 0$ .

Next we obtain equation for  $\rho_{\text{bulk}} = \rho_b^{(0)}$ . To this end, consider (31) at the order  $\mu^0$  and pass to the limit  $z \to \infty$ . After we rewrite the resulting equation in the original coordinate system we recover the Fokker–Planck equation for  $\rho_{\text{bulk}}$ :

(37) 
$$\partial_t \rho_{\text{bulk}} + \nabla_{\mathbf{r}} \cdot (\mathbf{u} \rho_{\text{bulk}}) + \partial_{\varphi} (T \rho_{\text{bulk}}) = D_{\text{rot}} \partial_{\varphi}^2 \rho_{\text{bulk}}.$$

Representation (9) with  $\psi_{\text{wall}}$  and  $\rho_{\text{bulk}}$  satisfying (36) and (37), respectively, is valid if  $\mathbf{u} \cdot \mathbf{n}|_{\Gamma} > 0$  for all  $-\pi \leq \varphi < \pi$ . In this case, active rods accumulate at the wall, but they cannot leave the wall. On the other hand, due to the rotational diffusion, active rods in experiments (for example, those described by system (43)–(44)) may leave the wall and be reinjected into the bulk. In this case, one needs an additional boundary layer term in the representation (27) (with an additional scale different from 1 and  $\mu$ ) which will capture active rods at wall  $\Gamma$  with  $\mathbf{u} \cdot \mathbf{n} \approx 0$ . It is similar to "parabolic boundary layers" in vanishing diffusion limit in elliptic equations; these boundary layers introduce two new scales  $\mu^{1/3}$  and  $\mu^{2/3}$ , and these terms are constructed at boundary points where characteristics of the limiting hyperbolic equation are tangential to the boundary; see section 2.7.5 in [17]; see also [41]. In this work, the formula for  $\chi$  in (10), the flux of reinjected active rods, i.e., with  $\mathbf{r} \in \Gamma$ ,  $\mathbf{u} \cdot \mathbf{n}|_{\Gamma} \approx 0$ , and  $\frac{\mathrm{d}}{\mathrm{d}t}\mathbf{u} \cdot \mathbf{n}|_{\Gamma} < 0$ , is derived from the conservation of total density:

$$\frac{\mathrm{d}}{\mathrm{d}t} \left[ \int_{-\pi}^{\pi} \int_{\Omega} \rho_{\text{bulk}} \, \mathrm{d}\mathbf{r} \mathrm{d}\varphi + \int_{\Gamma} \int_{\varphi_{1}}^{\varphi_{2}} \psi_{\text{wall}} \, \mathrm{d}\varphi \mathrm{d}s \right] = 0.$$

Adding terms with flux  $\chi$  to the right-hand side of (37) we derive system (10).

**5. Numerical example.** In this section, we provide a numerical example to illustrate the relation between a specific individual based model for an active rod and corresponding kinetic approaches discussed above.

We assume that the wall  $\Gamma$  coincides with x-axis, i.e.,  $\Gamma = \{(x,y) : y = 0\}$ , and the active rod's probability distribution function does not depend on x (see Figure 1, left). Drag  $\boldsymbol{u}$  exerted on an active rod is the sum of two components: a background shear flow  $\boldsymbol{u}_{\mathrm{BG}} = (\dot{\gamma}y, 0)$  and self-propulsion  $v_{\mathrm{prop}}(\cos\varphi, \sin\varphi)$ . The vertical component u of drag velocity  $\boldsymbol{u}$  and torque T exerted on an active rod are defined as follows:

$$u(y,\varphi) = u(\varphi) = v_{\text{prop}} \sin \varphi, \quad T(y,\varphi) = T(\varphi) = -0.5\dot{\gamma}(1 - \cos(2\varphi)).$$

Note that since the background shear flow  $u_{\rm BG}$  has zero y-component it does not enter the formula for vertical drag u. The expression for T follows from (45) from section 6.1 with  $T = \Phi_{\rm BG}$ . Parameters  $v_{\rm prop} = 0.2$  and  $\dot{\gamma} = 1.0$  are self-propulsion speed and shear rate, respectively.

First, we perform Monte Carlo simulations for the individual based model for an active rod with vertical component y(t) of location r(t) and orientation angle  $\varphi$  swimming in  $\Omega = \{y > 0\}$ :

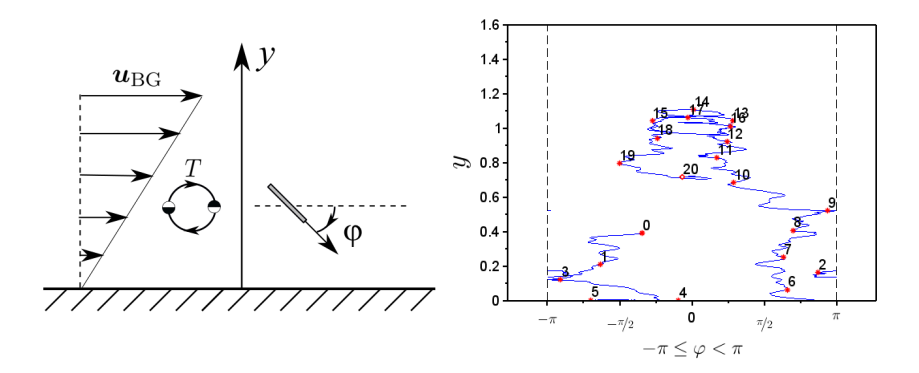


FIG. 1. Left: sketch of an active rod with orientation  $\varphi$  in xy-plane; x-axis represents the wall; straight arrows illustrate background shear flow  $\mathbf{u}_{BG}$ ; circle shows how the background torque  $T(\varphi)$  acts on the active rod; arrows along the circle show that equation  $\dot{\varphi} = T(\varphi)$  has two semistable states  $\varphi = 0$  and  $\varphi = -\pi$ . Right: a sample trajectory in  $\varphi$ y-plane for  $0 \le t \le 20$ . Red dots with numbers along trajectories indicate trajectory points at corresponding integer time moments.

(38) 
$$\dot{y} = u(\varphi), \quad \dot{\varphi} = T(\varphi) + \sqrt{2D_{\text{rot}}}\zeta,$$

where  $\zeta$  is the white noise with  $\langle \zeta(t), \zeta(t') \rangle = \delta(t-t')$  and  $D_{\text{rot}}$  is the rotational diffusion coefficient. The following "overdamped" collision-with-wall rule for y(t) = 0 is imposed:

(39) 
$$\dot{y}|_{y(t)=0} = \begin{cases} 0, & \sin \varphi \le 0, \\ u(\varphi), & \sin \varphi > 0, \end{cases} \quad \dot{\varphi}|_{y(t)=0} = T(\varphi) + \sqrt{2D_{\text{rot}}}\zeta.$$

This collision rule means that the active rod does not move if it is oriented towards the wall, i.e., downward,  $\sin \varphi(t) \leq 0$ . Regardless of whether it points downward or upward, the active rod's orientation  $\varphi$  is governed by the same equation as in the bulk. Note that, as is often done in applications (see, e.g., [31]) we neglect inertia and translational diffusion in the individual based model.

Next, we compare results of Monte Carlo simulations for individual based model (38)–(39) with the initial boundary value problem derived in Theorem 2.1 from section 3, consisting of the Fokker–Planck equation for probability distribution function  $\rho(t,y,\varphi)$ ,

(40) 
$$\partial_t \rho + v_{\text{prop}} \sin \varphi \partial_y \rho - 0.5 \dot{\gamma} \partial_\varphi ((1 - \cos(2\varphi))\rho) = D_{\text{tr}} \partial_y^2 \rho + D_{\text{rot}} \partial_\varphi^2 \rho,$$

and the no-flux boundary condition,

(41) 
$$D_{\rm tr}\partial_y \rho = v_{\rm prop}\rho \sin \varphi \quad \text{for} \quad y = 0.$$

The translation diffusion coefficient is chosen to be small,  $D_{\rm tr} = 0.05$ .

Finally, we simulate (10), derived as the limit  $D_{\rm tr} \to 0$  in (40)–(41).

To simulate the individual based model (38)–(39), the forward Euler–Maruyama method was used with time step  $\mathrm{d}t=10^{-3}$  and number of realizations (for Monte Carlo simulations)  $R=5\cdot 10^4$ . For Fokker–Planck problems (40)–(41) and (10), we used the finite difference explicit method with upwind scheme to take into account direction of fluxes; spatial and angular steps are  $\mathrm{d}y=0.05$  and  $\mathrm{d}\varphi=\pi/20$ , whereas the time step is  $\mathrm{d}t=\mathrm{d}y\,\mathrm{d}\varphi/10.0$ .

A sample trajectory obtained from simulating (38)–(39) for 0 < t < 20 is depicted in Figure 1, right. This trajectory is drawn in  $\varphi y$ -plane, and rod locations within this plane at integer moment of times are marked by red dots while the value of the corresponding moment of time is written above each dot. The trajectory demonstrates typical behavior of an active rod swimming at a wall. After collision with the wall, (t=4), the rod attaches to the wall (it still can swim in x direction) and reorients under background shear decreasing orientation angle  $\varphi$  to  $\varphi = -\pi$ , and then detaches from the wall ( $t \approx 5.5$ ). Note that swimming with orientation  $\varphi$  close to  $\pm \pi$  with background flow given by  $\mathbf{u}_{\rm BG} = (\dot{\gamma} y, 0)$  means that the active rod swims upstream, that is, exhibits negative rheotaxis.

For Monte Carlo simulations of (38)–(39) we chose initial location y and orientation angle  $\varphi$  to be random with uniform distributions in intervals 0.25 < y < 1.25 and  $-3\pi/4 < \varphi < -\pi/4$ , respectively. The corresponding initial condition for both probability distribution functions  $\rho^{\rm I}$ , solution of the Fokker–Planck equation (40) with no flux boundary condition (41), and  $\rho^{\rm II}$ , given by two-scale expansion (28)–(29) with  $\mu = D_{\rm tr} = 0.05$  and terms  $\rho_{\rm bulk}$  and  $\psi_{\rm wall}$  solving system (10), are

(42) 
$$\begin{cases} \frac{2}{\pi}, & \frac{1}{4} < y < \frac{5}{4}, -\frac{3\pi}{4} < \varphi < -\frac{\pi}{4}, \\ 0 & \text{otherwise.} \end{cases}$$

The initial condition (42) is shown in Figure 2, upper left.

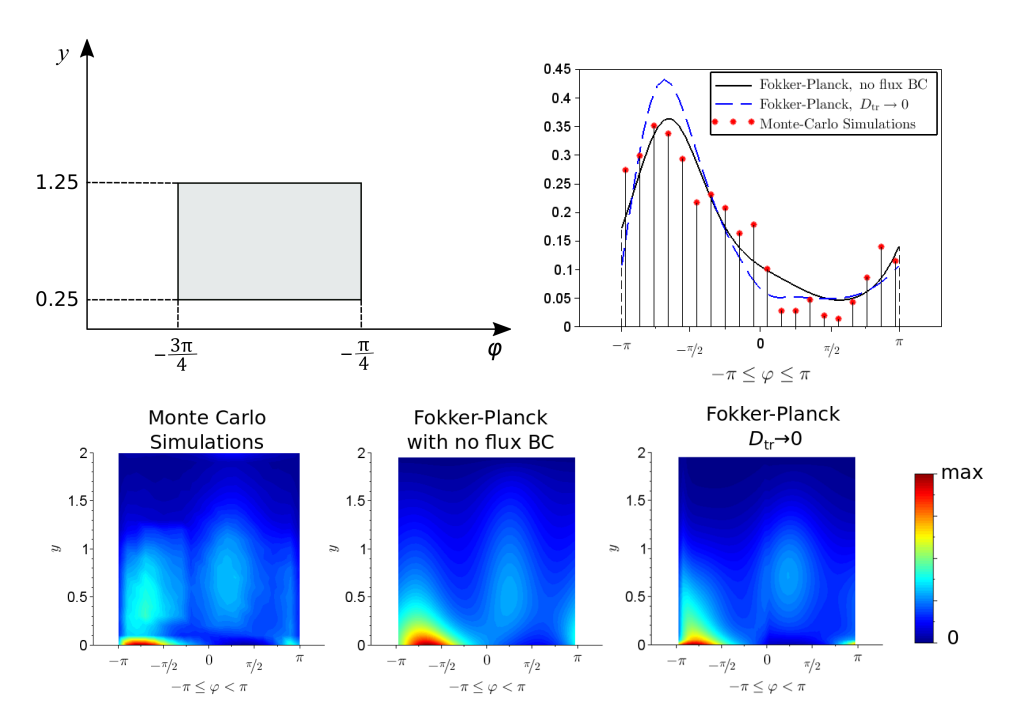


FIG. 2. Upper left: support  $\{0.25 < y < 1.25, \sin\varphi < -\sqrt{2}/2\}$  of probability distribution function  $\rho$  at t=0; upper right: angular distribution for t=10 of accumulated particles at wall from Monte Carlo simulations (red dots), Fokker–Planck problem (40)–(41) (solid line), and two-scale expansions (28) (dashed line); lower figures: $(\varphi, y)$ -histogram obtained from simulations of (38)–(39) (left);  $(\varphi, y)$ -distribution obtained from solution of (40)–(41) (center);  $(\varphi, y)$ -distribution obtained from two-scale expansions (28)–(29) with  $\mu=0.05$  and  $\rho_{bulk}$ ,  $\psi_{wall}$  solving (10) (right). All lower plots are computed for t=10.

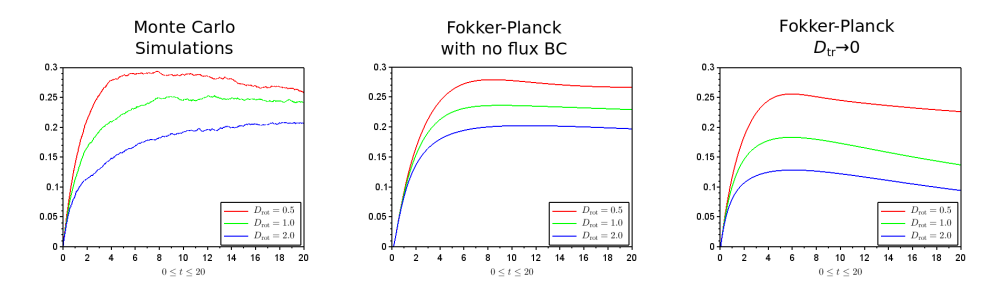


FIG. 3. Probability that active rod is accumulated at wall for 0 < t < 20 from Monte Carlo simulations (left), Fokker-Planck boundary value problem (40)-(41) (center), and two-scale expansion (28)-(29) with  $\mu = 0.05$  and  $\rho_{bulk}$ ,  $\psi_{wall}$  solving (10) (right).

Results of numerical simulations are depicted in Figures 2 and 3. The behavior of solutions of all the three problems—Monte Carlo simulations of individual based model (38)–(39), Fokker–Planck equation (40) with no flux boundary condition (41), and two-scale expansion (28)–(29) with  $\mu=D_{\rm tr}=0.05$  and terms  $\rho_{\rm bulk}$  and  $\psi_{\rm wall}$  solving system (10)—is qualitatively similar. Distributions of location y and orientation  $\varphi$  concentrate at  $y\approx 0$  and  $\varphi\approx -\pi$  (Figure 2, lower row). These plots illustrate wall accumulation  $y\approx 0$  and negative rheotaxis  $\varphi\approx -\pi$ . In this numerical example, initial condition (42) is chosen such that active rods initially point towards the wall, so the wall accumulation is somewhat enforced. Nevertheless, if the domain is confined from all sides, which is a generic situation, an active rod reaches the wall with a high probability and spends a nonzero time at the wall reorienting before being detached. Therefore, the wall accumulation of active rods in bounded domains necessarily occurs, and the numerical example in this section investigates the situation when a population of active rods approach a wall.

We also analyzed the active rod distribution inside boundary layer  $\mathcal{L} := \{0 \leq y < 0.2\}$  (accumulated active rods). Comparison of angular distributions at t = 10, obtained from the three approaches, is given in Figure 2, upper right, and the probability of swimming inside boundary layer  $\mathcal{L}$ , as a function of time 0 < t < 20, is depicted in Figure 3. All the three methods show active rod accumulation increases up to a moment 3 < t < 5 (depending on the value of rotational diffusion coefficient  $D_{\text{rot}}$ ; see Figure 3) and a peak of angular orientations forms close to  $\phi = -\pi$  (see Figure 2, upper right). However, the third method slightly underestimates the probability of swimming inside the boundary layer  $\mathcal{L}$  for larger values of  $D_{\text{rot}}$  (specifically, for  $D_{\text{rot}} = 2.0$ ). This underlines the subtlety, described in the paragraph after (37), of the multiscale expansion for  $\rho$  with respect to  $\mu$  and presence of the scales additional to 1 and  $\mu^{-1}$  in (27). Rigorous analysis of the limit  $\mu \to 0$  of the solution to problem (7)–(8) and explicit convergence estimates are left for our future work.

## 6. Individual based model and Fokker–Planck equation for an active rod with inertia.

**6.1.** Individual based model for an active rod with inertia. In this section we present equations governing the motion of an active rod in the domain  $\Omega \subset \mathbb{R}^2$  with nonempty boundary  $\Gamma = \partial \Omega$ . The rod is assumed to be a nondeformable one-dimensional segment of length  $\ell$  swimming in a viscous fluid. At each moment of time t the rod is characterized by the location of its center of mass r(t) and the orientation angle  $\varphi(t)$ , so that the unit vector  $p(\varphi) = (\cos \varphi, \sin \varphi)$  with  $\varphi = \varphi(t)$  determines the orientation of the active rod. Equations for r(t) and  $\varphi(t)$  are

(43) 
$$m \ddot{\mathbf{r}} = \eta_1 \ell \left( \mathbf{u}_{\mathrm{BG}}(\mathbf{r}) - \dot{\mathbf{r}} \right) + F_{\mathrm{thrust}} \mathbf{p}(\varphi) + \sqrt{2D_{\mathrm{tr}}} \zeta_1,$$

(44) 
$$I_{\text{rod}}\ddot{\varphi} = \eta_2 \ell^2 (\Phi_{\text{BG}}(\mathbf{r}, \varphi) - \dot{\varphi}) + \sqrt{2D_{\text{rot}}} \zeta_2.$$

Here  $\rho_0$  is the density of the rod, so  $m = \rho_0 \ell$  is its mass;  $I_{\rm rod} = \rho_0 \ell^3/12$  is the moment of inertia of the rod around the center of mass;  $\eta_1$  and  $\eta_2$  are material constants related to the background fluid viscosity. Function  $\boldsymbol{u}_{\rm BG}(\boldsymbol{r})$  is the velocity of the background flow at point  $\boldsymbol{r}$ . We assume that the background flow is not affected by the active rod. Thus,  $\boldsymbol{u}_{\rm BG}$  satisfies the homogeneous Stokes equation in  $\Omega$ :

$$-\eta_1 \Delta \boldsymbol{u}_{\mathrm{BG}} + \nabla p = 0,$$
$$\nabla \cdot \boldsymbol{u}_{\mathrm{BG}} = 0.$$

 $F_{\rm thrust}$  is the magnitude of the thrust force (the self-propulsion force);  $D_{\rm tr}$  and  $D_{\rm rot}$  are translational and rotational diffusion coefficients, respectively;  $\zeta_1$  and  $\zeta_2$  are uncorrelated white noises with intensities  $\langle \zeta_i(t), \zeta_i(t') \rangle = \delta(t-t')$ , i=1,2. Function  $\Phi_{\rm BG}(\boldsymbol{r},\varphi)$  can be understood as the proportionality coefficient defining the torque due to the background flow exerted on the unit rod at location  $\boldsymbol{r}$ , with orientation angle  $\varphi$  and zero angular velocity, and  $\Phi_{\rm BG}(\boldsymbol{r},\varphi)$  is given by

(45) 
$$\Phi_{\mathrm{BG}}(\boldsymbol{r},\varphi) = (\mathbb{I} - \boldsymbol{p}\boldsymbol{p}^{\mathrm{T}})\nabla \boldsymbol{u}_{\mathrm{BG}}(\boldsymbol{r})\boldsymbol{p} \cdot \mathbf{e}_{\varphi}, \quad \mathbf{e}_{\varphi} = (-\sin\varphi,\cos\varphi).$$

Equation (43) is the force balance for the active rod, and this equation reads as follows. There are three forces exerted on the active rod: (i) the viscous drag force which is proportional to the relative velocity of the active rod with respect to the background flow, (ii) the self-propulsion force directed always along the orientation of the active rod, and (iii) the random (Brownian) force. Equation (44) is the torque balance for the active rod which implies that there are two torques reorienting the active rod: viscous and random torques. Here we assume that the self-propulsion force does not affect orientation of the active rod.

The system (43)–(44) can be written in the following general form:

$$\frac{\mathrm{d}\boldsymbol{r}}{\mathrm{d}t} = \boldsymbol{v}$$

(47) 
$$\frac{\mathrm{d}\boldsymbol{v}}{\mathrm{d}t} = \frac{1}{\varepsilon}(\boldsymbol{u}(\boldsymbol{r},\varphi,t) - \boldsymbol{v}) + \sqrt{2D_{\mathrm{tr}}}\,\zeta_1,$$

(48) 
$$\frac{\mathrm{d}\varphi}{\mathrm{d}t} = \omega,$$

(49) 
$$\frac{\mathrm{d}\omega}{\mathrm{d}t} = \frac{1}{\varepsilon} (T(\mathbf{r}, \varphi, t) - \omega) + \sqrt{2D_{\mathrm{rot}}} \zeta_2.$$

Here  $u(\mathbf{r}, \varphi, t)$  and  $T(\mathbf{r}, \varphi, t)$  are given smooth and bounded functions, and  $\varepsilon$  is a small parameter.

Next, we describe the rule of collision of the active rod and the wall  $\Gamma$ . At time of a collision,  $t_{\text{coll}}$ , an instantaneous force (an impulse) is exerted on the rod, and this force is directed normal to  $\Gamma$  (see Figure 4):

$$F_{\text{coll}} = -m\sigma \boldsymbol{n} \,\delta(t - t_{\text{coll}}),$$

where n is the outward normal vector and  $\sigma$  will be determined below. One can formally add the force  $F_{\text{coll}}$  to the right-hand side of (43). This translates into the following collision rule for velocities:

$$(50) v' = v - \sigma n,$$

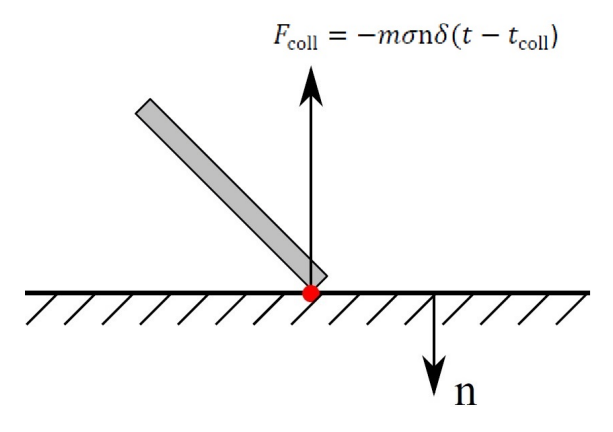


Fig. 4. A force exerted on the active rod due to a collision with the wall.

where  $\mathbf{v} = \dot{\mathbf{r}}(t_{\rm coll} - 0)$  and  $\mathbf{v}' = \dot{\mathbf{r}}(t_{\rm coll} + 0)$  are velocities before and after the collision, respectively. The force  $F_{\rm coll}$  is exerted at the front of the active rod which touches the wall  $\Gamma$ . This implies that the active rod has an additional torque (in the right-hand side of (44)) due to the collision, which equals to  $-m\sigma \frac{\ell}{2} (\mathbf{p} \times \mathbf{n})\delta(t - t_{\rm coll})$ , and thus the collision rule for angular velocities is

(51) 
$$\omega' = \omega - \frac{6}{\ell} \sigma(\boldsymbol{p} \times \boldsymbol{n}) \cdot \mathbf{e}_z,$$

where  $\omega = \dot{\varphi}(t_{\rm coll} - 0)$  and  $\omega' = \dot{\varphi}(t_{\rm coll} + 0)$  are angular velocities before and after the collision, respectively, and  $e_z = (0, 0, 1)$  is the unit vector orthogonal to the plane containing domain  $\Omega$ .

To completely describe the collision rule, the value of parameter  $\sigma$  needs to be determined. To this end, we assume that the collision is perfectly elastic, that is, the kinetic energy does not change in time of the collision:

(52) 
$$\frac{1}{2}m\boldsymbol{v}^2 + \frac{1}{2}I_{\text{rod}}\omega^2 = \frac{m}{2}(\boldsymbol{v} - \sigma\boldsymbol{n})^2 + \frac{I_{\text{rod}}}{2}\left(\omega - \frac{6}{\ell}\sigma\left(\boldsymbol{p}\times\boldsymbol{n}\right)\cdot\mathbf{e}_z\right)^2.$$

Expanding the right-hand side of (52) we get the formula for  $\sigma$ :

(53) 
$$\sigma = \frac{2(\boldsymbol{v} \cdot \boldsymbol{n}) + \ell\omega(\boldsymbol{p} \times \boldsymbol{n}) \cdot e_z}{1 + 3|\boldsymbol{p} \times \boldsymbol{n}|^2}.$$

Remark 2. We can extend our consideration to imperfect elastic conditions, that is, we may assume that a part of energy is lost in time of collision:

(54) 
$$\frac{1}{2}mv'^{2} + \frac{1}{2}I_{\text{rod}}\omega'^{2} = \epsilon \left\{ \frac{1}{2}mv^{2} + \frac{1}{2}I_{\text{rod}}\omega^{2} \right\},$$

where  $0 \le \epsilon \le 1$  is coefficient of restitution which measures how elastic the collision is: if it is 1, the collision is perfectly elastic; if  $\epsilon = 0$ , the collision is perfectly inelastic.

Proposition 3. Let C be the linear operator (a  $3 \times 3$  matrix)

(55) 
$$C: (\boldsymbol{v}, \omega) \mapsto \left(\boldsymbol{v} - \sigma \, \boldsymbol{n}, \omega - \frac{6}{\ell} \sigma(\boldsymbol{p} \times \boldsymbol{n}) \cdot e_z\right)$$

with  $\sigma$  from (53). Then

$$|\det \mathcal{C}| = 1.$$

*Proof.* Denote  $v_{\mathbf{n}} := \boldsymbol{v} \cdot \boldsymbol{n}$  and  $v_{\tau} := \boldsymbol{v} \cdot \boldsymbol{\tau}$  ( $\boldsymbol{\tau}$  is the unit tangent vector on  $\Gamma$ ). We also represent  $\sigma$  as follows:

$$\sigma = Av_n + B\omega$$
, where  $A = \frac{2}{1 + 3|\boldsymbol{p} \times \boldsymbol{n}|^2}$  and  $B = \frac{\ell(\boldsymbol{p} \times \boldsymbol{n}) \cdot e_z}{1 + 3|\boldsymbol{p} \times \boldsymbol{n}|^2}$ .

In addition, we introduce angle  $\theta$  between vectors  $\mathbf{p}$  and  $\mathbf{n}$ . Note that  $\sin \theta = (\mathbf{p} \times \mathbf{n}) \cdot \mathbf{e}_z$ .

Then the operator  $\mathcal{C}$  can be represented by

$$\mathcal{CV} = \begin{bmatrix} 1 & 0 & 0 \\ 0 & 1-A & -B \\ 0 & -\frac{6}{\ell}\sin\theta\,A & 1-\frac{6}{\ell}\sin\theta\,B \end{bmatrix} \begin{bmatrix} v_\tau \\ v_\mathrm{n} \\ \omega \end{bmatrix}.$$

Finally, we compute  $\det \mathcal{C}$ :

$$\det \mathcal{C} = \begin{vmatrix} 1 - A & -B \\ -\frac{6}{\ell} \sin \theta A & 1 - \frac{6}{\ell} \sin \theta B \end{vmatrix} = -1.$$

Thus, the proof of proposition is complete.

6.2. Fokker–Planck equation for an active rod with inertia. For active rods whose motion inside domain  $\Omega$  is described by (46)–(49), the Fokker–Planck equation is

(57) 
$$\partial_{t}\tilde{f}_{\varepsilon} + \boldsymbol{v} \cdot \nabla_{\boldsymbol{r}}\tilde{f}_{\varepsilon} + \frac{1}{\varepsilon}\nabla_{\boldsymbol{v}} \cdot \left((\boldsymbol{u} - \boldsymbol{v})\tilde{f}_{\varepsilon} - \varepsilon D_{\mathrm{tr}}\nabla_{\boldsymbol{v}}\tilde{f}_{\varepsilon}\right) + \omega \partial_{\varphi}\tilde{f}_{\varepsilon} + \frac{1}{\varepsilon}\partial_{\omega}\left((T - \omega)\tilde{f}_{\varepsilon} - \varepsilon D_{\mathrm{rot}}\partial_{\omega}\tilde{f}_{\varepsilon}\right) = 0.$$

The unknown function  $\tilde{f}_{\varepsilon}(t, \boldsymbol{r}, \boldsymbol{v}, \varphi, \omega)$  is the probability distribution function of the active rod's location  $\boldsymbol{r} \in \Omega$ , translational velocity  $\boldsymbol{v} \in \mathbb{R}^2$ , orientation angle  $\varphi \in [-\pi, \pi)$ , and angular velocity  $\omega \in \mathbb{R}$ .

The collision rule of the active rods with the wall  $\Gamma$  is given by (50)–(51). The rule translates into the following boundary conditions for  $\tilde{f}_{\varepsilon}$ :

(58) 
$$\boldsymbol{v}\tilde{f}_{\varepsilon}\cdot\boldsymbol{n}=\boldsymbol{v}'\tilde{f}'_{\varepsilon}\cdot(-\boldsymbol{n}),\ \boldsymbol{r}\ \mathrm{on}\ \Gamma,$$

where  $\tilde{f}'_{\varepsilon} = \tilde{f}_{\varepsilon}(t, \boldsymbol{r}, \boldsymbol{v}', \varphi, \omega')$  and the pair  $(\boldsymbol{v}', \omega')$  is given by collision rule (50)–(51).

Remark 3. The meaning of boundary condition (58) is as follows: the flux of incident active rods equal to the flux of reflected active rods. In other words, the flux is the same before and after collisions. Note that if one considers spherical particles with no preferred orientation (no  $\varphi$  and  $\omega$ ), then the collision rule is  $\mathbf{v}' = \mathbf{v} - 2(\mathbf{v} \cdot \mathbf{n})\mathbf{n}$ , and (58) is reduced in this case to equality of probability distribution functions  $f_{\varepsilon} = f'_{\varepsilon}$ . This boundary condition is used in many works where particles are assumed to be spherical; see, e.g., [12, 22, 23]. We point out here that imposing such boundary conditions (equality of probability distribution functions instead of fluxes as in (58)) for active rods leads to violation of both the mass conservation and the energy relation.

In this work we are interested in the limit  $\varepsilon \to 0$ . Following [12, 22, 23], to obtain a meaningful limit we first rescale  $\tilde{f}_{\varepsilon}$ :

$$f_{\varepsilon}(t, \boldsymbol{r}, \boldsymbol{v}, \varphi, \omega) = \tilde{f}_{\varepsilon}(t, \boldsymbol{r}, \varepsilon \boldsymbol{v}, \varphi, \varepsilon \omega).$$

Then the Fokker–Planck equation for the rescaled probability distribution function  $f_{\varepsilon}$  has the following form:

(59) 
$$\partial_{t} f_{\varepsilon} + \frac{1}{\varepsilon} \boldsymbol{v} \cdot \nabla_{\boldsymbol{r}} f_{\varepsilon} + \frac{1}{\varepsilon^{2}} \nabla_{\boldsymbol{v}} \cdot ((\varepsilon \boldsymbol{u} - \boldsymbol{v}) f_{\varepsilon} - D_{\mathrm{tr}} \nabla_{\boldsymbol{v}} f_{\varepsilon}) + \frac{1}{\varepsilon} \omega \partial_{\varphi} f_{\varepsilon} + \frac{1}{\varepsilon^{2}} \partial_{\omega} \left( (\varepsilon T - \omega) f_{\varepsilon} - D_{\mathrm{rot}} \partial_{\omega} f_{\varepsilon} \right) = 0$$

with boundary condition (58) for  $f_{\varepsilon}$ .

## REFERENCES

- [1] R. Baker, J. Kauffman, A. Laskar, O. Shklyaev, M. Potomkin, H. Shum, Y. Cruz-Rivera, I. Aronson, A. Balazs, and A. Sen, Fight the flow: Collective rheotaxis of artificial swimmers in confined systems, Nanoscale, 11 (2018), pp. 10944–10951.
- [2] H. Berg and L. Turner, Chemotaxis of bacteria in glass capillary arrays. Escherichia coli, motility, microchannel plate, and light scattering, Biophys. J., 58 (1990), pp. 919–930.
- [3] A. Berke, L. Turner, H. Berg, and E. Lauga, Hydrodynamic attraction of swinning microorganisms by surfaces, Phys. Rev. Lett., 101 (2008), 038102.
- [4] R. CAFLISCH AND G. PAPANICOLAOU, Dynamic theory of suspensions with Brownian effects, SIAM J. Appl. Math., (1983), pp. 885–906.
- [5] A. CAVAGNA AND I. GIARDINA, Bird flocks as condensed matter, Annu. Rev. Condensed Matter Phys., 5 (2014), pp. 183–2017.
- [6] A. DECOENE, S. MARTIN, AND B. MAURY, Microscopic modelling of active bacterial suspensions, Math. Model. Nat. Phenom., 6 (2011), pp. 98–129.
- [7] J. ELGETI, R. WINKLER, AND G. GOMPPER, Physics of microswimmers single particle motion and collective behavior: A review, Rep. Progr. Phys., 78 (2015), 056601.
- [8] B. EZHILAN AND D. SAINTILLAN, Transport of a dilute active suspension in pressure-driven channel flow, J. Fluid Mech., 777 (2015), pp. 480–522.
- [9] P. Frymier, R. Ford, H. Berg, and P. Cummings, Three-dimensional tracking of motile bacteria near a solid planar surface, Proc. Natl. Acad. Sci. USA, 92 (1995), pp. 6195–6199.
- [10] H. C. Fu, T. R. Powers, and R. Stocker, Bacterial rheotaxis, Proc. Natl. Acad. Sci. USA, 109 (2012), pp. 4780–4785.
- [11] R. Glassey, The Cauchy Problem in Kinetic Theory, SIAM, Philadelphia, PA, 1996.
- [12] T. GOUDON, P.-E. JABIN, AND A. VASSEUR, Hydrodynamic limits for Vlasov-Stokes equations: Part I: Light particles regime, Indiana Univ. Math. J., 53 (2004), pp. 1495–1513.
- [13] B. M. HAINES, I. S. ARANSON, L. BERLYAND, AND D. A. KARPEEV, Effective viscosity of bacterial suspensions: A three-dimensional pde model with stochastic torque, Commun. Pure Appl. Anal., 11 (2010), pp. 19–46.
- [14] B. M. Haines, A. Sokolov, I. S. Aranson, L. Berlyand, and D. A. Karpeev, A threedimensional model for the effective viscosity of bacterial suspensions, Phys. Rev. E, 80 (2009), 041922.
- [15] J. HERNANDEZ-ORTIZ, C. STOLTZ, AND M. GRAHAM, Transport and collective dynamics in suspensions of confined swimming particles, Phys. Rev. Lett., 95 (2005), 204501.
- [16] J. HILL, O. KALKANCI, J. MCMURRY, AND H. KOSER, Hydrodynamic surface interactions enable Escherichia coli to seek efficient routes to swim upstream, Phys. Rev. Lett., 98 (2007), 068101.
- [17] M. HOLMES, Introduction to Perturbation Methods, Springer Science & Business Media, New York, NY, 2012.
- [18] A. KAISER, A. PESHKOV, A. SOKOLOV, B. TEN HAGEN, H. LÖWEN, AND I. S. ARANSON, Transport powered by bacterial turbulence, Phys. Rev. Lett., 112 (2014), 158101.
- [19] Y. KATZ, K. TUNSTRØM, C. IOANNOU, C. HUEPE, AND I. COUZIN, Inferring the structure and dynamics of interactions in schooling fish, Proc. Natl. Acad. Sci. USA, 108 (2011), pp. 18720–18725.

- [20] H. LÓPEZ, J. GACHELIN, C. DOUARCHE, H. AURADOU, AND E. CLÉMENT, Turning bacteria suspensions into superfluids, Phys. Rev. Lett., 115 (2015), 028301.
- [21] M. MARCHETTI, J. JOANNY, S. RAMASWAMY, T. LIVERPOOL, J. PROST, M. RAO, AND R. SIMHA, Hydrodynamics of soft active matter, Rev. Modern Phys., 85 (2013), 1143.
- [22] A. MELLET AND A. VASSEUR, Global weak solutions for a Vlasov-Fokker-Planck/Navier-Stokes system of equations, Math. Models Methods Appl. Sci., 17 (2007), pp. 1039–1063.
- [23] A. MELLET AND A. VASSEUR, Asymptotic analysis for a Vlasov-Fokker-Planck/compressible Navier-Stokes system of equations, Comm. Math. Phys., 281 (2008), pp. 573-596.
- [24] G. Mino, T. Mallouk, T. Darnige, M. Hoyos, J. Dauchet, J. Dunstan, R. Soto, Y. Wang, A. Rousselet, and E. Clement, Enhanced diffusion due to active swimmers at a solid surface, Phys. Rev. Lett., 106 (2011), 048102.
- [25] S. MOTSCH AND E. TADMOR, A new model for self-organized dynamics and its flocking behavior, J. Stat. Phys., 144 (2011), 923.
- [26] J. PALACCI, S. SACANNA, A. ABRAMIAN, J. BARRAL, K. HANSON, A. GROSBERG, D. PINE, AND P. CHAIKIN, Artificial rheotaxis, Sci. Adv., 1 (2015), e1400214.
- [27] W. F. PAXTON, K. C. KISTLER, C. C. OLMEDA, A. SEN, S. K. ST. ANGELO, Y. CAO, T. E. MALLOUK, P. E. LAMMERT, AND V. H. CRESPI, Catalytic nanomotors: Autonomous movement of striped nanorods, J. Amer. Chem. Soc., 126 (2004), pp. 13424–13431.
- [28] F. PERUANI, A. DEUTSCH, AND M. BÄR, Nonequilibrium clustering of self-propelled rods, Phys. Rev. E, 74 (2006), 030904.
- [29] E. PINCE, S. VELU, A. CALLEGARI, P. ELAHI, S. GIGAN, G. VOLPE, AND G. VOLPE, Disorder-mediated crowd control in an active matter system, Nat. Commun., 7 (2016), 10907.
- [30] G. Popkin, The physics of life, Nat. News, 529 (2016), 16.
- [31] M. POTOMKIN, A. KAISER, L. BERLYAND, AND I. ARANSON, Focusing of active particles in a converging flow, New J. Phys., 19 (2017), 115005.
- [32] M. POTOMKIN, M. TOURNUS, L. BERLYAND, AND I. ARANSON, Flagella bending affects macroscopic properties of bacterial suspensions, J. Roy. Soc. Interface, 14 (2017), 20161031.
- [33] S. RAMASWAMY, The mechanics and statistics of active matter, Annu. Rev. Condensed Matter Phys., 1 (2010), pp. 323–345.
- [34] M. RAMIA, D. TULLOCK, AND N. PHAN-THIEN, The role of hydrodynamic interaction in the locomotion of microorganisms, Biophys. J., 65 (1993), pp. 755-778.
- [35] L. ROTHSCHILD, Non-random distribution of bull spermatozoa in a drop of sperm suspension, Nature, 198 (1963), 1221.
- [36] J. RUBINSHTEIN AND J. KELLER, Particle distribution functions in suspensions, Phys. Fluids A Fluid Dyn., 1 (1989), pp. 1632–1641.
- [37] S. RYAN, A. SOKOLOV, L. BERLYAND, AND I. ARANSON, Correlation properties of collective motion in bacterial suspension, New J. Phys., 15 (2013), 105021.
- [38] D. SAINTILLAN AND M. SHELLEY, Orientational order and instabilities in suspensions of selflocomoting rods, Phys. Rev. Lett., 99 (2007), 058102.
- [39] A. SOKOLOV, I. ARANSON, J. KESSLER, AND R. GOLDSTEIN, Concentration dependence of the collective dynamics of swimming bacteria, Phys. Rev. Lett., 98 (2007), 158102.
- [40] K. Tunstrøm, Y. Katz, C. Ioannou, C. Huepe, M. Lutz, and I. Couzin, Collective states, multistability and transitional behavior in schooling fish, PLoS Comput. Biol., 9 (2013), p. e1002915.
- [41] A. VAN HARTEN, On an elliptic singular perturbation problem, in Ordinary and Partial Differential Equations, W. M. Everitt and B. D. Sleeman, eds., Springer-Verlag, Berlin, 1976, pp. 485–495.
- [42] M. VIGEANT, R. FORD, M. WAGNER, AND L. TAMM, Reversible and irreversible adhesion of motile Escherichia coli cells analyzed by total internal reflection aqueous fluorescence microscopy, Appl. Environ. Microbiol., 68 (2002), pp. 2794–2801.
- [43] H. WENSINK AND H. LÖWEN, Emergent states in dense systems of active rods: From swarming to turbulence, J. Phys. Condensed Matter, 24 (2012), 464130.
- [44] X. Wu and A. Libchaber, Particle diffusion in a quasi-two-dimensional bacterial bath, Phys. Rev. Lett., 84 (2000), 3017.
- [45] J. Yuan, D. Raizen, and H. Bau, Propensity of undulatory swimmers, such as worms, to go against the flow, Proc. Natl. Acad. Sci. USA, 112 (2015), pp. 3606–3611.